

# Spectroscopic classification, variability and SED of the *Fermi*-detected CSS 3C 286: the radio-loudest NLS1 galaxy?

Su Yao<sup>\*</sup> and S. Komossa<sup>†</sup>

Max-Planck-Institut für Radioastronomie, Auf dem Hügel 69, 53121 Bonn, Germany

Accepted XXX. Received 2020; in original form

## ABSTRACT

3C 286 is a well-known calibrator source in radio astronomy. It is also one of very few compact steep-spectrum sources (CSS) detected in  $\gamma$ -rays. Here, we perform a detailed spectroscopic and variability analysis and present the first quasi-simultaneous optical to X-ray spectral energy distribution in order to reveal physical mechanisms which dominate its emission at different wavelengths, and arrive at a reliable optical source classification. The first main result of our study reveals several pitfalls when applying simple broad- or narrow-line Seyfert 1 (BLS1 or NLS1) classification criteria which only look at the [O III]-H $\beta$  complex. [O III] and H $\beta$  can be dominated by the same outflow components, in which case FWHM(H $\beta$ ) is no reliable classification criterion, and extinction by intrinsic or intervening material can make the highest-velocity H $\beta$  component undetectable. After careful combination of all information from UV-optical spectra along with multi-wavelength data, we confirm that 3C 286 can be classified as NLS1 galaxy, with line properties and SMBH mass (of order  $10^8 M_{\odot}$  and accreting near the Eddington limit) close to the BLS1 regime, making it an important borderline object. The quasi-simultaneous SED taken with *Swift* shows a sharp rise in the optical-UV, implying the presence of a strong accretion-disk component with EUV excess, consistent with emission-line diagnostics. Finally, we report the discovery of X-ray variability of 3C 286, plausibly dominated by jet emission, and variable by at least a factor  $\sim 4$ . This result suggests to exercise caution when using 3C 286 as radio calibrator in high-resolution radio VLBI observations.

**Key words:** galaxies: active – galaxies: nuclei – galaxies: jets – galaxies: Seyfert – quasars: supermassive black holes – quasars: individual: 3C 286

## 1 INTRODUCTION

The majority of sources detected by the *Fermi* mission in  $\gamma$ -rays are classical blazars with their jets pointing at us and with massive host galaxies (Abdollahi et al. 2020). However, *Fermi* has also detected small numbers of other classes of galaxies and active galactic nuclei (AGN), including a few starburst galaxies (e.g., Peng et al. 2016; Griffin et al. 2016), nearby Seyfert galaxies (e.g., Hayashida et al. 2013), broad-line radio galaxies (e.g., Kataoka et al. 2011; Brown & Adams 2012), and compact-steep-spectral (CSS) sources (Massaro et al. 2015; Abdollahi et al. 2020). In particular, *Fermi* detected several narrow-line type 1 quasars and narrow-line Seyfert 1 galaxies for the first time in  $\gamma$ -rays (e.g., Abdo et al. 2009; Paliya et al. 2018; Yao et al. 2019; review by Komossa 2018), confirming the existence of relativistic jets in these sources independently inferred from radio studies (Komossa et al. 2006a; Yuan et al. 2008; Foschini et al. 2015).

Narrow-line type 1 AGN (quasars and their lower-luminosity equivalents of Seyfert galaxies; from now on collectively referred to as NLS1 galaxies) are AGN with exceptional properties and at an extreme end of a set of correlations between the H $\beta$  line width and other observables (Boroson & Green 1992; Sulentic et al. 2000;

Zhou et al. 2006; Grupe et al. 2010; Xu et al. 2012). They are characterized by narrow Balmer lines of the broad-line region (BLR) with full-width-at-half-maximum (FWHM)  $< 2200 \text{ km s}^{-1}$ , weak [O III] and strong Fe II emission, steep soft X-ray spectra, show strong outflow components, enhanced star formation activity, and are rapidly growing their less massive central supermassive black holes (SMBHs; review by Komossa 2008).

Only 7% of all NLS1 galaxies were found to be radio-loud (preferentially the narrow-line type 1 quasars; Komossa et al. 2006a) and only  $\sim 16$  of them have been detected in  $\gamma$ -rays (Table 1 of Komossa 2018). As their multi-wavelength properties are characteristically different from classical blazars, their study is important for understanding the disk-jet connection in a previously unexplored parameter regime, and since the known systems are few, it is of great interest to identify more cases.

The quasar 3C 286 was identified as a CSS (Peacock & Wall 1982) and is exceptional in being one out of only  $\sim 5$  CSSs significantly detected in  $\gamma$ -rays with *Fermi*<sup>1</sup>. It is detected at a significance of  $\sim 6.8\sigma$  and a Bayesian-based association probability of 98.5% (Abdollahi et al. 2020). Zhang et al. (2020) re-analyzed the 11-year *Fermi* data, and independently confirmed the source identification.

<sup>1</sup> See evidence for the *Fermi* detection of another CSS-NLS1, RXJ2314.9+2243, but at faint emission levels so its  $\gamma$ -ray identification still needs to be confirmed (Komossa et al. 2015).

<sup>\*</sup> E-mail: syao@mpifr-bonn.mpg.de

<sup>†</sup> E-mail: astrokomossa@gmx.de

**Table 1.** Log of SDSS-BOSS, *Chandra* ACIS-S and *Swift* XRT and UVOT observations of 3C 286.

Mission	Band	Obs-date	MJD	Exp. (s)
SDSS		2005-04-07	53467	2220
SDSS-BOSS		2013-02-14	56337	3603
<i>Chandra</i> ACIS-S	0.3-10 keV	2013-02-26	56349	2004
<i>Swift</i> XRT	0.3-10 keV	2020-08-16	59077	2018
		2020-08-21	59082	1374
<i>Swift</i> UVOT	v	2020-08-16	59077	162
		2020-08-21	59082	104
	b	2020-08-16	59077	162
		2020-08-21	59082	104
	u	2020-08-16	59077	162
		2020-08-21	59082	104
	w1	2020-08-16	59077	323
		2020-08-21	59082	208
	m2	2020-08-16	59077	485
		2020-08-21	59082	373
	w2	2020-08-16	59077	648
		2020-08-21	59082	416

3C 286 is a widely used calibrator source in radio astronomy<sup>2</sup> because of its very stable radio emission and polarization for decades (Perley & Butler 2013a,b). Its radio emission is compact at sub-arcsecond scales, with a jet and a counter-jet (e.g. Wilkinson et al. 1979; Simon et al. 1980; Cotton et al. 1997; Fomalont et al. 2000; An et al. 2017) and some outer emission extending to  $\sim 3.8''$  (Spencer et al. 1989; Akujor & Garrington 1995; An et al. 2004). The viewing angle of its inner jet on tens of parsec scales was estimated at  $48^\circ$  based on the apparent proper-motion speed (An et al. 2017).

Because its  $H\beta$  emission was not easily accessible from ground-based spectroscopy given its redshift of  $z = 0.85$ , its AGN type remained uncertain, and both an intermediate-type broad-line Seyfert 1 (BLS1) (Véron-Cetty & Véron 2010) or a NLS1 classification (Yao 2016; Berton et al. 2017; Liao & Gu 2020) was suggested. Here, we critically investigate the optical spectral classification of 3C 286 based on its full optical-UV emission-line spectrum along with tight multi-wavelength constraints on intrinsic absorption, evaluate the X-ray variability of special interest with regard to its radio-calibrator status, and present the first simultaneous optical-UV-X-ray spectral energy distribution (SED) of 3C 286.

We use a cosmology (Wright 2006) with  $H_0=70 \text{ km s}^{-1} \text{ Mpc}^{-1}$ ,  $\Omega_M=0.3$  and  $\Omega_\Lambda=0.7$  throughout this paper.

## 2 DATA ANALYSIS AND RESULTS

### 2.1 SDSS

In the course of the Sloan Digital Sky Survey (SDSS; York et al. 2000) 3C 286 was observed on April 7, 2005 (MJD 53467) and February 14, 2013 (MJD 56337), respectively. The later spectrum from the SDSS-BOSS survey (Dawson et al. 2013) covers a wider spectral range of  $\sim 3600\text{--}10400 \text{ \AA}$  which corresponds to  $\sim 1950\text{--}5600 \text{ \AA}$  at rest frame of the object. We retrieved the calibrated 1D spectra of both observations from the SDSS archive and corrected them for Galactic extinction with  $E(B - V) = 0.011 \text{ mag}$  (Schlafly & Finkbeiner

2011) and an  $R_V = 3.1$  extinction law. Then the spectra were transformed into the source rest frame at  $z = 0.850$  provided by the SDSS spectroscopic pipeline.

To inspect the variations between the spectra at the two epochs, we scale the spectrum taken in 2005 to match the  $[\text{O III}]\lambda 3727$  flux of the 2013 spectrum, obtained from direct integration of the continuum-subtracted line profile. So we assume that the flux of  $[\text{O III}]\lambda 3727$  does not vary on timescales of years. Then the scaled 2005 spectrum is subtracted from the 2013 spectrum to obtain the spectral variation. The spectrum taken in 2013 is shown in Figure 1(a) and the spectral variation is shown in Figure 1(b). As can be seen, there is only a minor change in the continuum while the emission lines of 3C 286 at the two epochs are nearly constant. Thus, we only perform a spectral fitting on the 2013 spectrum.

The spectral fitting is based on IDL routines in the MPFIT package (Markwardt 2009), which performs a  $\chi^2$  minimization using the Levenberg-Marquardt method. Firstly, we fit the  $[\text{O III}]\text{-H}\beta\text{-H}\gamma$  region using data in windows of  $[4720, 5300] \text{ \AA}$ ,  $[4160, 4630] \text{ \AA}$ ,  $[3990, 4080] \text{ \AA}$ ,  $[3900, 3950] \text{ \AA}$ ,  $[3760, 3850] \text{ \AA}$ ,  $[3500, 3690] \text{ \AA}$ . These windows are chosen in order to mask all the possible emission line regions except  $H\beta 4861$ ,  $H\gamma 4340$ ,  $[\text{O III}]\lambda\lambda 4959, 5007$  and the  $\text{Fe II}$  multiplet underneath.

A pseudo continuum consisting of a single power law and  $\text{Fe II}$  multiplets modelled by templates of Véron-Cetty et al. (2004) is adopted. Each of the  $[\text{O III}]\lambda\lambda 4959, 5007$  doublet is modelled with two Gaussians, one for the core, the other for the possible blue-shifted wings. Both of the doublets are constrained to have the same profile and redshift during the fitting, and the flux ratio of  $[\text{O III}]\lambda 4959$  to  $[\text{O III}]\lambda 5007$  is fixed to the theoretical value of 1:2.98. The  $H\beta$  and  $H\gamma$  emission lines are modelled with three Gaussians. One of the Gaussians represents the narrow component originating from the narrow-line region (NLR), and is constrained to have the same profile and redshift as the core of  $[\text{O III}]\lambda 5007$ . The combination of the other two Gaussians represents the broad component presumably originating from the BLR. The flux ratio of the narrow  $H\gamma$  to  $H\beta$  is fixed at 0.46:1 assuming Case B (Osterbrock & Ferland 2006). The broad  $H\beta$  and  $H\gamma$  lines are constrained to have the same profile and redshift, while their fluxes are set to be free parameters. We do not see any visible signature of  $[\text{O III}]\lambda 4363$ , so this line is not included in the model. The best-fit models of  $H\beta$  and  $[\text{O III}]\lambda\lambda 4959, 5007$  are displayed in Figure 1(c). We also try to use a Lorentzian profile instead of a double-Gaussian to model the broad component of  $H\beta$ , which gives an equally good fit result.

The  $\text{Mg II}$  region is fitted separately from the  $[\text{O III}]\text{-H}\beta\text{-H}\gamma$  region. We use the data in the windows of  $[2200, 2295] \text{ \AA}$ ,  $[2355, 2400] \text{ \AA}$ ,  $[2485, 2640] \text{ \AA}$ ,  $[2690, 3100] \text{ \AA}$ ,  $[3170, 3400] \text{ \AA}$ ,  $[3610, 3700] \text{ \AA}$  in order to mask the emission line regions listed in Table 2 of Vanden Berk et al. (2001) except for the  $\text{Mg II}\lambda\lambda 2796, 2803$  doublet and the  $\text{Fe II}$  multiplet underneath. Similarly, a single power law plus  $\text{Fe II}$  multiplet modelled by the template in Tsuzuki et al. (2006) are used to represent a pseudo-continuum. Each line of the doublet is modelled with one broad and one narrow component. The broad component is a truncated five-parameter Gauss-Hermite profile (Wang et al. 2009) and the narrow component is a single Gaussian. Both broad components of the doublet are assumed to have the same profile and redshift, and their flux ratio is fixed at 1.2:1 assuming an entirely thermalized gas for simplicity (Laor et al. 1997). The narrow components of the doublet are constrained following the same prescription, additionally with their  $\text{FWHM} \leq 900 \text{ km s}^{-1}$ .

Then we subtract the best-fit model of the  $[\text{O III}]\text{-H}\beta\text{-H}\gamma$  and  $\text{Mg II}$  region from the spectrum, and fit  $[\text{Ne V}]\lambda 3426$ ,  $[\text{O II}]\lambda 3727$ ,  $[\text{Ne III}]\lambda 3870$  and  $\text{He II}\lambda 4686$  in the residuals, as these lines are visi-

<sup>2</sup> <https://casa.nrao.edu/docs/cookbook/>

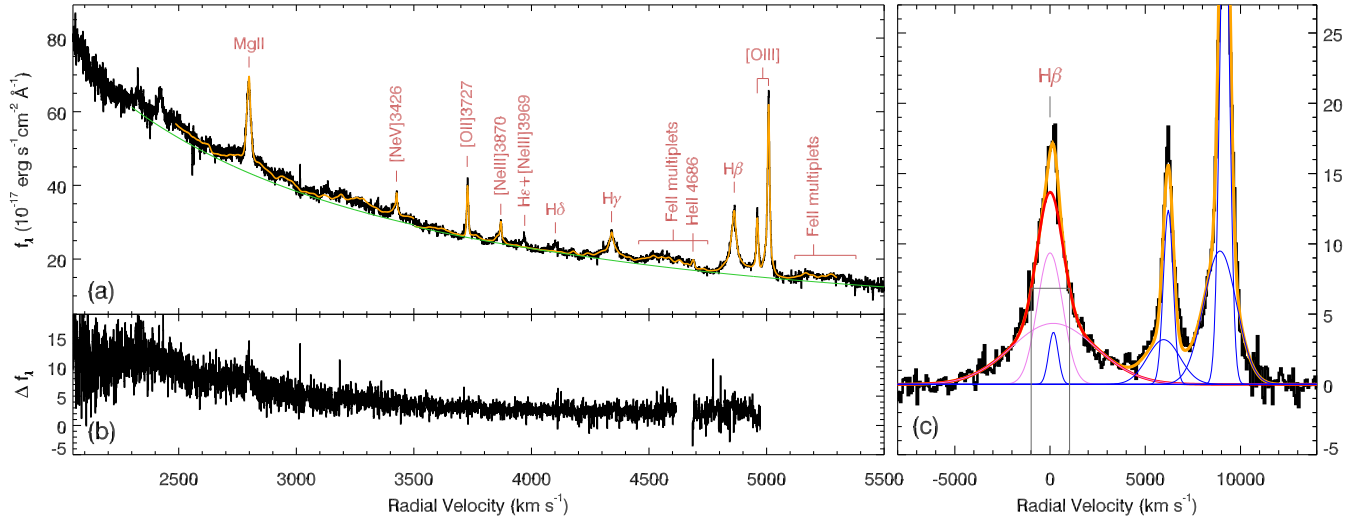


**Figure 1.** (a) The rest-frame SDSS-BOSS spectrum (black) of 3C 286 after correction for Galactic extinction. The orange curves represent the combination of the best-fit models described in Section 2.1. (b) The residuals of subtracting the 2005 SDSS spectrum from the 2013 SDSS-BOSS spectrum. (c) The best-fit decomposition of the  $H\beta$ -[O III] complex. The black curve represents the 2013 SDSS-BOSS spectrum subtracted by the pseudo-continuum model. The red line represents the broad component of  $H\beta$  of which the FWHM is shown by a gray rectangle, and the blue lines represent the narrow component of  $H\beta$  and [O III]  $\lambda\lambda 4959, 5007$ . The orange line represents the sum of the models. The pink curves represent the double-Gaussian profiles composing the broad  $H\beta$ .

bly detected and isolated, and easy to be measured. The [O II]  $\lambda 3727$  and He II  $\lambda 4686$  are modelled by single Gaussian profiles, while [Ne V]  $\lambda 3426$  and [Ne III]  $\lambda 3870$  are decomposed into two Gaussian profiles similarly as [O III]  $\lambda 5007$  considering possible blue-shifted wings. The fit results are shown in Figure 2. [O II]  $\lambda 3727$  is well fitted by a single Gaussian which has a slightly larger line width compared to the core component of [O III]  $\lambda 5007$  (Table 2). The core components of [Ne V]  $\lambda 3426$ , [Ne III]  $\lambda 3870$  and [O III]  $\lambda 5007$  have nearly the same redshifts as [O II]  $\lambda 3727$ . We also notice very faint excess emission implying that there might be a slight blue wing component in [O II]  $\lambda 3727$  which, however, is not statistically significant in the present data.

To estimate the uncertainties of the fitting, we follow the same approach as in Shen et al. (2011). We generate 1000 mock spectra by adding Gaussian noise to the real spectrum flux densities using flux density errors, and fit the mock spectra with the same fitting procedure described above. The uncertainties are determined from the 68% range of the distributions of fitting results from mock spectra. All the measured quantities of the real emission lines and their uncertainties are listed in Table 2.

## 2.2 Neil Gehrels *Swift* observatory

In order to measure the X-ray spectrum, search for X-ray variability on long (years) and short (days) timescales, and to obtain the first simultaneous optical–UV–X-ray SED of 3C 286, we have obtained two observations with the Neil Gehrels *Swift* observatory (*Swift* hereafter; Gehrels et al. 2004) in 2020 (Table 1; Target-Id 13644, PI: S. Komossa).

### 2.2.1 *Swift* XRT

The *Swift* X-ray telescope (XRT; Burrows et al. 2005) was operating in photon counting mode (Hill et al. 2004) with exposure times of 1–2 ks each (Table 1). During the two observations, the countrates of 3C 286 were low and constant. For the spectral analysis, we extracted the source photons within a circle of radius  $47''$ , while the

**Table 2.** Emission-line results.

Line (1)	FWHM (2)	Flux (3)	Velocity (4)
$H\beta_{\text{broad}}$	$2001 \pm 222$	$119.3 \pm 5.8$	...
$H\beta_{\text{broad, lorentzian}}$	$1858 \pm 124$	$133.6 \pm 2.7$	$93 \pm 19$
$H\beta_{\text{broad, comp1}}$	$1556 \pm 246$	$46.8 \pm 8.3$	$136 \pm 38$
$H\beta_{\text{broad, comp2}}$	$5209 \pm 1052$	$72.5 \pm 4.9$	$-38 \pm 267$
$H\beta_{\text{narrow}}$	... <sup>a</sup>	$6.9 \pm 2.6$	... <sup>a</sup>
$H\gamma_{\text{broad}}$	... <sup>b</sup>	$42.6 \pm 2.6$	... <sup>b</sup>
[O III] $\lambda 5007$	$683 \pm 20$	$133.2 \pm 1.8$	...
[O III] $\lambda 5007_{\text{core}}$	$572 \pm 29$	$71.5 \pm 5.1$	$-43 \pm 11$
[O III] $\lambda 5007_{\text{wing}}$	$1953 \pm 151$	$61.7 \pm 4.4$	$192.3 \pm 69$
He II $\lambda 4686$	$842 \pm 295$	$5.8 \pm 1.0$	$-63 \pm 93$
[Ne III] $\lambda 3870$	$746 \pm 90$	$18.8 \pm 1.4$	...
[Ne III] $\lambda 3870_{\text{core}}$	$556 \pm 76$	$5.9 \pm 1.1$	$-3 \pm 32$
[Ne III] $\lambda 3870_{\text{wing}}$	$2398 \pm 407$	$12.9 \pm 1.9$	$579 \pm 156$
[O II] $\lambda 3727$	$715 \pm 30$	$23.7 \pm 0.8$	0.0
[Ne V] $\lambda 3426$	$731 \pm 216$	$14.7 \pm 1.0$	...
[Ne V] $\lambda 3426_{\text{core}}$	$476 \pm 234$	$3.7 \pm 3.1$	$-5.4 \pm 48$
[Ne V] $\lambda 3426_{\text{wing}}$	$1747 \pm 351$	$11.0 \pm 3.2$	$204 \pm 350$
Mg II $\lambda 2796_{\text{broad}}$	$2064 \pm 257$	$54.2 \pm 4.5$	$54 \pm 57$
$R_{4570}^a$		$0.76 \pm 0.04$	

**Note.** Column (2): The FWHM of each line, not corrected for instrumental broadening, in units of  $\text{km s}^{-1}$ . Column (3): The flux of each line in units of  $10^{-16} \text{erg s}^{-1} \text{cm}^{-2}$ . Column (4): The relative velocity of each line with respect to [O II]  $\lambda 3727$  in units of  $\text{km s}^{-1}$ .

<sup>a</sup> The profile and redshift are tied to [O III]  $\lambda 5007$  core component.

<sup>b</sup> The profile and redshift are tied to  $H\beta$  broad component.

<sup>c</sup> The relative strength of Fe II,  $R_{4570} \equiv \text{Fe II } \lambda 4570 / H\beta_{\text{total}}$ , where Fe II  $\lambda 4570$  is calculated by integrating the Fe II multiplet from  $4434 \text{\AA}$  to  $4684 \text{\AA}$ .

background was determined in an annulus with inner and outer radius of  $60''$  and  $100''$  respectively. As 3C 286 is faint in X-rays, we combined the data sets of the two single observations in order to carry out the spectral fits. We created new ancillary response files (arfs) by adding the arfs of the single spectra weighted by their exposure time using the `FTOOL` command `addarf`. The co-added X-ray spectra in the

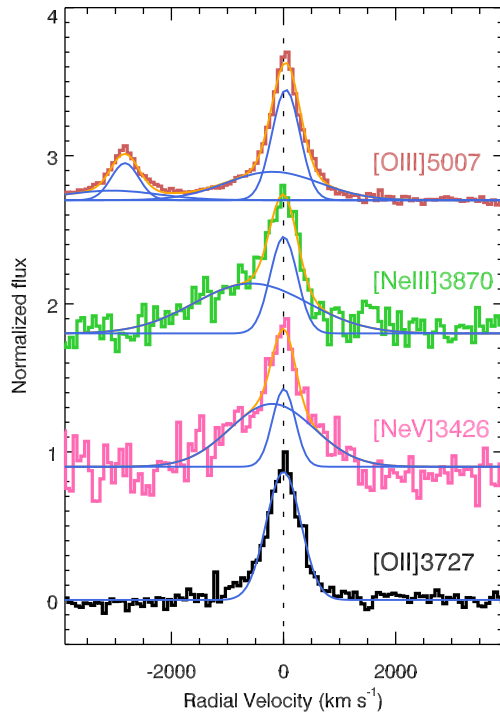


**Figure 2.** The velocity profiles of [O III] $\lambda\lambda$ 4959, 5007, [Ne III] $\lambda$ 3870 and [Ne V] $\lambda$ 3426 with respect to [O II] $\lambda$ 3727. The blue curves represent the best-fit decomposition. The dotted vertical line denotes the velocity centroid of [O II] $\lambda$ 3727. A blue wing is present in the high-ionization lines.

**Table 3.** The results of single power law model fitted to the X-ray spectra.

	$\Gamma_X$	$A_{1\text{keV}}^a$	$f_{0.3-10\text{keV}}^b$	$C/\text{dof}$
<i>Swift</i>	$1.8 \pm 0.5$	$2.2^{+0.5}_{-0.6}$	$1.4^{+0.6}_{-0.5}$	4.6/3
<i>Chandra</i>	$2.1 \pm 0.2$	$12.2^{+1.2}_{-1.1}$	$6.4 \pm 0.6$	10.4/11
<i>Chandra</i> <sup>c</sup>	$2.2 \pm 0.2$	$12.6^{+1.2}_{-1.1}$	$7.4^{+0.7}_{-0.6}$	11.4/11

**Note.** Galactic absorption with  $N_{\text{H}}^{\text{Gal}} = 1.11 \times 10^{20} \text{ cm}^{-2}$  is always included in the model during the fitting.

<sup>a</sup> The normalization of the power law at the observed frame at 1 keV in units of  $10^{-5} \text{ photons keV}^{-1} \text{ cm}^{-2} \text{ s}^{-1}$ .

<sup>b</sup> The Galactic absorption-corrected flux in units of  $10^{-13} \text{ erg s}^{-1} \text{ cm}^{-2}$ .

<sup>c</sup> An extra absorption at redshift  $z = 0.692$  with column density of  $N_{\text{H}} = 2 \times 10^{21} \text{ cm}^{-2}$  and 10% solar abundances is added.

band 0.3–10 keV have only 38 counts in total. Thus the spectra were re-binned to have 7 counts in each bin and then analyzed based on  $C$ -statistics (Cash 1979) using the software package XSPEC (version 12.11.1; Arnaud 1996). A single power law with Galactic absorption of  $N_{\text{H}}^{\text{Gal}} = 1.11 \times 10^{20} \text{ cm}^{-2}$  (HI4PI Collaboration et al. 2016) fits the data well. The spectrum is flat with photon index  $\Gamma_X = 1.8 \pm 0.5$  ( $C/\text{dof} = 4.64/3$  using  $C$ -statistics). The absorption-corrected flux is  $F_{0.3-10\text{keV}} = 1.4^{+0.6}_{-0.5} \times 10^{-13} \text{ erg s}^{-1} \text{ cm}^{-2}$ , corresponding to a luminosity of  $4.9 \times 10^{44} \text{ erg s}^{-1}$ .

### 2.2.2 *Swift* UVOT

Two observations of 3C 286 were obtained with the UV-optical telescope (UVOT; Roming et al. 2005) in all six filters (Table 1) in order to obtain SED information. For each observation, data in each filter were co-added using the task *uvotimsum*. Source counts in all filters were then extracted in a circular region of radius  $5''$ , while the back-

ground was selected in a nearby source-free region of radius  $15''$ . The background-corrected counts were then converted into fluxes based on the latest calibration as described in Poole et al. (2008) and Breeveld et al. (2010), using the task *uvotsource* and CALDB (version 20201026). We checked the derived  $b - v$  colours and find that they are out of the range over which the conversions used by *uvotsource* are applicable. Thus we fit the UV/optical photometric data with a log-parabolic model, and calculate new conversion factors, as well as the Galactic extinction correction, by folding the best-fit log-parabolic model with the effective area of each filter following Raiteri et al. (2010). The final flux is obtained using the new conversion factors.

### 2.3 *Chandra* data

We have also analyzed archival *Chandra* data in order to search for flux and/or spectral variability in comparison with the *Swift* data. 3C 286 was observed by *Chandra* ACIS-S for an exposure time of 2 ks on February 26 2013 as a Guest Observer program (Table 1; observation ID 15006, PI: J. Kuraszkiewicz). The data are reduced using CIAO (version 4.12) and CALDB (version 4.9.2.1). The level 2 event file is created following the standard procedure. Source detection performed using the *celldetec* task reveals the center for the X-ray source at R.A. =  $13^{\text{h}}31^{\text{m}}08.31^{\text{s}}$ , Dec. =  $+30^{\circ}30'33.0''$ , with an offset of only  $0.3''$  from the optical position of 3C 286. No other X-ray source is detected near 3C 286 within  $\sim 2'$ . We have searched for extended X-ray emission, but find that 95% of the photons are within  $2''$ , consistent with a point source.

For spectral analysis, we extract source photons from a circular region with radius of  $6''$ . The background is determined in an annulus region with inner and outer radius of  $10''$  and  $30''$ , respectively. As there are only 130 net counts, the spectrum is grouped to have at least 10 counts per bin and the  $C$ -statistics is adopted for minimization. The spectrum is well fit by a single power law with absorption fixed at the Galactic value and a photon index  $\Gamma_X = 2.1 \pm 0.2$  ( $C/\text{dof} = 10.4/11$  using  $C$ -statistics). No excess absorption is required (Figure 3). The photon index agrees with the value measured with *Swift* within errors, while the absorption-corrected flux  $F_{0.3-10\text{keV}} = (6.4 \pm 0.6) \times 10^{-13} \text{ erg s}^{-1} \text{ cm}^{-2}$  varied by a factor of  $\sim 4$  compared to *Swift* observation. Since a low-metallicity damped Ly $\alpha$  absorption system with  $N_{\text{H}} \sim 2 \times 10^{21} \text{ cm}^{-2}$  was found at  $z = 0.692$  in front of 3C 286 (e.g., Brown & Roberts 1973; Meyer & York 1992), we also test an additional intervening absorption by  $N_{\text{H}} = 2 \times 10^{21} \text{ cm}^{-2}$  with 10% solar metallicity at redshift of  $z = 0.692$  (see Section 3.1.1), but find a worse fit. The parameters of models for both *Swift* and *Chandra* are listed in Table 3.

### 2.4 Archival data

For an assessment of the IR variability and determination of the broad-band SED of 3C 286, first, we have inspected data from the *Single Exposure Source Table* of WISE/NeOWISE (Wright et al. 2010; Mainzer et al. 2011) and find no evidence for significant variability on both short and long time-scales. We then used the average measurements from combined images reported in the AllWISE Source Catalog (Cutri et al. 2013). In addition, the infrared data from 2MASS (Skrutskie et al. 2006) and data from *Spitzer* (Cleary et al. 2007) are included to build the broad-band SED. We have also added the *Fermi* spectrum in 100 MeV–10 GeV based on the measurements from the *Fermi* Fourth Source Catalog (Abdollahi et al. 2020), the SDSS-BOSS UV-optical spectrum (Section 2.1) and the core radio fluxes taken from Aslanian et al. (1968), Laing & Peacock

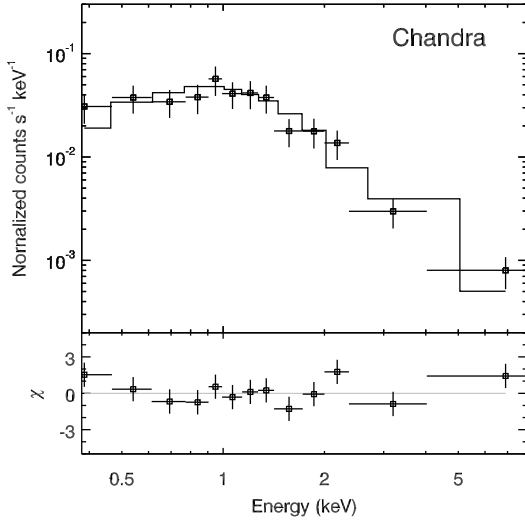


**Figure 3.** Power-law model fit to the *Chandra* ACIS-S spectrum of 3C 286 (upper panel), and the residuals (lower panel) of the power-law fit to the spectrum.

(1980), Kuehr et al. (1981), Gregory & Condon (1991), Becker et al. (1995), Waldram et al. (1996), Laurent-Muehleisen et al. (1997), Meisenheimer et al. (2001), Chandra et al. (2004), Curran et al. (2004), Cohen et al. (2007), Gabányi et al. (2007), Mantovani et al. (2009), Chen & Wright (2009), Mao et al. (2010), Jenness et al. (2010), Richards et al. (2011), Gold et al. (2011) and Agudo et al. (2014). The SED of 3C 286 is shown in Figure 4. For comparison, we plot the SEDs of two  $\gamma$ -ray detected NLS1 galaxies at similar redshift, J0946+1017 ( $z = 1.004$ , Yao et al. 2019) and J1222+0413 ( $z = 0.966$ , Yao et al. 2015). The model of J1222+0413’s SED taken from Yao et al. (2015) is also shown. As can be seen from Figure 4, compared to its optical/UV flux, 3C 286 is relatively weak in X-rays.

## 2.5 SMBH mass and Eddington ratio

We use three different methods of estimating BH mass. First, the SMBH mass  $M_{\text{BH}}$  can be estimated using the monochromatic continuum luminosity at  $5100 \text{ \AA}$ ,  $L_{5100}$ , and broad line width of  $H\beta$  from the Gauss fit, which are proxies for the radius and the virial velocity of the BLR, respectively (Vestergaard & Peterson 2006). Assuming that the emission of 3C 286 at  $5100 \text{ \AA}$  is fully due to the disk emission, we measure  $L_{5100} = 4.7 \times 10^{45} \text{ erg s}^{-1}$  and obtain  $M_{\text{BH}} = 2.3 \times 10^8 M_{\odot}$  (Equation 5 in Vestergaard & Peterson 2006). Then, we obtained an Eddington ratio, defined as the ratio of bolometric luminosity to Eddington luminosity, of  $\lambda_{\text{Edd}} = 1.6$  assuming a bolometric correction of  $k = 9.8$  (McLure & Dunlop 2004). Alternatively, considering the SED in the optical may be partly contributed by jet, we estimate  $L_{5100} = 1.6 \times 10^{45} \text{ erg s}^{-1}$  from the  $H\beta$  luminosity based on the relation given in Zhou et al. (2006), which leads to  $M_{\text{BH}} = 1.3 \times 10^8 M_{\odot}$  and  $\lambda_{\text{Edd}} = 1.0$ . Finally, a third method was used, based on the finding that the width  $\sigma$  of the  $[\text{O III}]\lambda 5007$  core component is a good surrogate for stellar velocity dispersion  $\sigma_*$ , where  $\sigma = \text{FWHM}/2.35$  (Nelson 2000; Komossa & Xu 2007). Employing the  $M_{\text{BH}}-\sigma_*$  relation (Ferrarese & Ford 2005), and based on our decomposition of  $[\text{O III}]\lambda 5007$ , we obtain  $M_{\text{BH}} = 4.3 \times 10^8 M_{\odot}$ . As above, we use  $L_{5100}$  as upper limit, and the same bolometric correction. Then,  $\lambda_{\text{Edd}} = 0.9$ .

All values of Eddington ratios from the 3 estimates above are consistent with the result  $\lambda_{\text{Edd}} = 0.9$  obtained from the SED modelling

in Zhang et al. (2020), indicating that 3C 286 is accreting near the Eddington limit.

## 3 DISCUSSION

### 3.1 AGN type from optical spectral classification

Because of its high redshift, the  $H\beta$  regime of 3C 286 was not easily accessible in the past. A spectrum by Gelderman & Whittle (1994) included  $H\beta$ , but the line was too noisy for measurements.  $H\alpha$  was detected by Hirst et al. (2003), but could not be resolved from neighbouring  $[\text{N II}]$  emission lines, with a total FWHM of  $\sim 2600 \text{ km s}^{-1}$ . 3C 286 was previously classified as a broad-line Seyfert 1.5 (Véron-Cetty & Véron 2010) and recently suggested to be of NLS1-type based on the presence of  $\text{Fe II}$  emission and an analysis of the  $H\beta$ - $[\text{O III}]$  complex of the SDSS-BOSS spectrum (e.g., Yao 2016; Berton et al. 2017; Liao & Gu 2020). Here, we present for the first time a full analysis of the UV-optical spectrum of 3C 286 from SDSS-BOSS including all detected emission lines. Given the unique properties of 3C 286, a reliable optical classification and an assessment of its variability is of great interest, and is essential in understanding the physical processes which govern its central engine. We discuss several classifications in turn:

#### 3.1.1 Absorbed intermediate-type broad-line Seyfert 1 galaxy

Given evidence for absorption along our line of sight, the question arises, whether the inner BLR of 3C 286 is highly obscured, such that we therefore miss a large part of the high-velocity component in  $H\beta$ , or whether the whole spectrum is affected by intervening dusty absorbers weakening it enough that the broadest component of  $H\beta$  becomes undetectable. Either would then imply, that the NLS1 classification is uncertain or even incorrect.

First, there is no evidence for *intrinsic* absorption/extinction in 3C 286. Its UV spectrum is very blue, the X-ray spectrum only requires Galactic absorption, and the  $\text{H I } 21 \text{ cm}$  absorption intrinsic to 3C 286 is exceptionally low with  $N_{\text{H}} < 0.052 \times 10^{20} \text{ cm}^{-2}$  (Grasha et al. 2019).

However, 3C 286 is well known for its damped  $\text{Ly}\alpha$  system (DLA) from an *intervening* absorber at  $z=0.692$  detected in UV spectra (e.g., Meyer & York 1992; Wolfe et al. 2008) and in  $\text{H I } 21 \text{ cm}$  absorption (e.g., Brown & Roberts 1973; Wolfe et al. 1976) with a column density of  $N_{\text{H}} \sim 2 \times 10^{21} \text{ cm}^{-2}$  (Cohen et al. 1994). The redshift and the very narrow Hydrogen absorption line width argues against an origin in 3C 286 itself. Detection of diffuse emission  $2.5''$  from 3C 286 suggests that the intervening absorber is a low surface brightness galaxy (Steidel et al. 1994). If the absorber of high column density was dusty, it would then significantly extinct the spectrum of 3C 286. However, measurements of multiple absorption lines from Hydrogen and different metals have shown, that both the metal abundances and also the dust to gas ratio of the absorber are very low. Meyer & York (1992) report a metallicity of only 6% solar and a dust-to-gas ratio of only 5% of that of the Galactic disk. A low dust content of the absorber was also inferred from the blue UV spectrum of 3C 286 (Boisse et al. 1998), and is consistent with larger sample studies of DLAs which find that these generally have low dust-to-gas ratios (Pei et al. 1991; Pettini et al. 1997).

We therefore conclude, that 3C 286 does not suffer strong extinction and that we measure the true  $H\beta$  width. As a note in passing, the low metallicity of the intervening absorber likely explains, why our X-ray spectral fit is consistent with Galactic absorption.

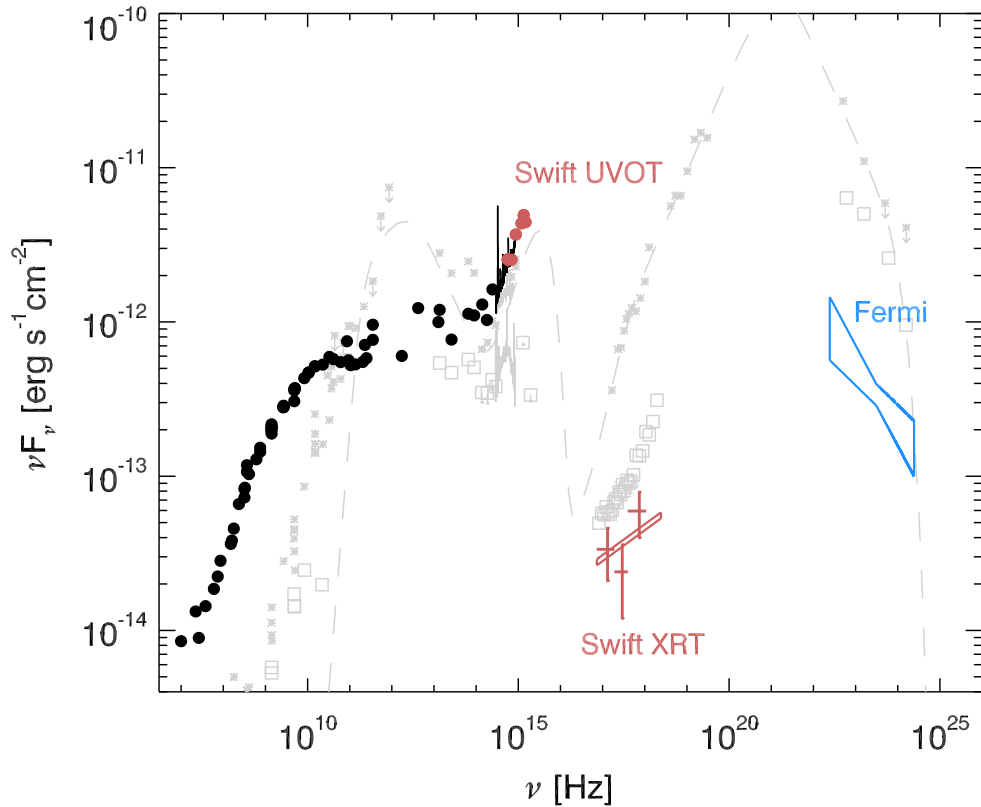


**Figure 4.** SED of 3C 286 based on our simultaneous *Swift* UVOT and XRT data (red) corrected for the Galactic absorption/extinction, along with non-simultaneous measurements from the *Fermi* Fourth Source Catalog (blue polygon), SDSS-BOSS spectroscopy (black curve) and the literature (filled black circles, see Section 2.4). The XRT data are re-binned for visual clarity and the red line represents the best-fit single power law. The SEDs of two  $\gamma$ -ray detected NLS1s at similarly high redshift, J0946+1017 (grey open squares) and J1222+0413 (grey asterisk), and the model for J1222+0413 (grey dashed line) are also plotted for comparison.

### 3.1.2 Starburst contribution

Given that Fe II emission complexes are also detected in some strong starbursts and that [O II] is strong in the optical spectrum, the question arises if starburst emission could be responsible for the Fe II complexes (e.g., Lipari et al. 1994). However, the profile of [O II] is similar to that of [O III]<sub>core</sub> arguing for a NLR origin, the lack of any detectable absorbing material argues against significant (gas-rich) starburst activity, and the IR emission should be dominated the synchrotron emission of the jet, not starburst-heated dust (see also Zhang et al. 2020).

### 3.1.3 NLS1 classification and outflow component

Taken at face value, line width measurements of H $\beta$  (Gauss or Lorentz) both imply a NLS1 classification of 3C 286 with  $\text{FWHM}(\text{H}\beta, \text{Gauss}) = 2001 \text{ km s}^{-1}$  and  $\text{FWHM}(\text{H}\beta, \text{Lorentz}) = 1858 \text{ km s}^{-1}$ . However, the width of H $\beta$  turns out to be very similar to broad [O III]. This is unusual and demands caution, as broad blue-shifted [O III] represents an outflow component, and the question is raised, whether H $\beta$  could be part of that same outflow and not representing the actual BLR, then just mimicking a NLS1 classification. However, other studies of outflows in NLS1 galaxies (e.g., Komossa et al. 2008; Berton et al. 2016a; Komossa et al. 2018) have shown, that only a negligible fraction of H $\beta$ -emitting matter (typically below the detection limit) and of other low-ionization gas

participates in the outflow, which is dominated by high-ionization transitions like [O III], [Ne III] and [Ne V]. The fact that Mg II at rest has a similar FWHM as H $\beta$  then argues for the fact that both transitions represent emission from a bona-fide BLR, confirming the NLS1 classification.

Finally, it has been suggested occasionally, that SMBH masses in NLS1 galaxies are higher than usually inferred, because of projection effects (a near face-on view onto a flattened BLR). While this effect was found not to play a major role in the majority of NLS1 galaxies (e.g., Section 7.2 of Komossa 2018 for a review), it could still be relevant in individual objects. However, 3C 286 is seen at a large angle of  $48^\circ$  (An et al. 2017) rather than face-on, and therefore projection effects do not play a significant role in narrowing down the observed line widths.

We therefore conclude, that 3C 286 can be reliably classified as NLS1-type, taken all evidence from the full optical spectrum combined with multi-wavelength data and especially the tight constraints on intrinsic absorption.

## 3.2 Radio-loudness

Since no excess absorption/extinction is detected in 3C 286, the optical flux measurement is reliable. Further, the bulk radio emission of 3C 286 is very compact. Therefore, the radio-loudness index defined as  $R = f_{5 \text{ GHz}}/f_{4400}$  in Kellermann et al. (1989) can be reliably measured. Using the SDSS  $g$ -magnitude of 17.33 mag and the

VLA 5 GHz flux of 7.5 Jy (Laurent-Muehleisen et al. 1997), we find  $\log R = 4.4$  after  $k$ -correction with radio spectral index  $\alpha_{\text{rad}} = -0.61$  (An et al. 2017) and optical spectral index  $\alpha_{\text{opt}} = -0.24$  from our SDSS spectrum analysis. If excluding the extended radio emission in the radio-index estimate, and instead using just the VLBI 4.9 GHz flux of 1.55 Jy of the brightest component of the core region on a scale of only  $\sim 50$  pc (An et al. 2017), then the radio loudness would still be  $\log R = 3.7$ . We also calculated the radio loudness at 1.4 GHz (which was often used in work on samples of NLS1 galaxies) using the FIRST 1.4 GHz flux of 15 Jy (Becker et al. 1995). This then gives  $\log R_{1.4\text{GHz}} = 4.7$ .

Therefore, 3C 286 is the radio-loudest NLS1 galaxy known; with a radio-loudness index even high when compared to broad-line radio galaxies (which show values between  $10^2$  to  $10^5$  (e.g., Sikora et al. 2007)).

### 3.3 Outflow component

3C 286 shows additional blue-wing components in its high-ionization emission lines [O III], [Ne III] and [Ne V] (Figure 2), implying that those lines arise in two different regions, a classical NLR and an outflow component. Blue wings are seen in a subset of other radio-quiet NLS1 (e.g., Sulentic et al. 2000; Grupe & Mathur 2004; Komossa et al. 2008) and radio-loud NLS1 galaxies (Berton et al. 2016a; Komossa et al. 2018), too. Drivers of the outflow can be jet-cloud interactions or radiation-pressure driving, for instance (Komossa 2018). Given that the jet in 3C 286 is rather inactive with constant polarization over decades, and given the high Eddington ratio of 3C 286 ( $L/L_{\text{Edd}} \sim 1$ ), we tentatively favor a large-scale outflow over local jet-cloud interactions.

### 3.4 Implications from emission-line ratios

Individual emission-line ratios are good estimators of the physical conditions of the line-emitting gas, and the shape of the SED. In our case, we can use the line ratio [O II]/[O III] as an estimator of the ionization parameter  $U$ , and the ratio of [Ne III]/[Ne V] as an indicator of the EUV SED (EUV excess or deficit), following Komossa et al. (2006b, their Section 3.2 and Figure 2). An intensity ratio  $\log([\text{O II}]/[\text{O III}]) = -0.75$  implies an ionization parameter of the NLR of  $\log U = -2.4$ . In combination with the measured intensity ratio  $\log([\text{Ne III}]/[\text{Ne V}]) = 0.11$ , this provides evidence for a soft excess in the EUV SED of 3C 286 (continuum “c4” in Figure 2b of Komossa et al. 2006b), consistent with the sharp rise we actually observe in the UV part of the SED of 3C 286 (Figure 4). We note in passing, that these parameters are very similar to the radio-loud NLS1 galaxy SDSS J172206.03+565451.6 (Komossa et al. 2006b).

### 3.5 SED

For the first time, we have measured with *Swift* a simultaneous optical–UV–X-ray SED of 3C 286 (Figure 4). The sharp rise in the optical-UV likely implies a strong accretion-disk contribution in the EUV (see also Zhang et al. 2020), as observed in other (radio-quiet) NLS1 galaxies, too. However, given the high redshift of the source, unfortunately the soft X-rays are redshifted out of the *Swift* band. Therefore, it can not be directly evaluated whether there is a soft X-ray excess which is commonly thought as a connection between the EUV emission from the accretion disk and the hard X-ray emission. On the other hand, the faintness of the hard X-rays can be seen from the comparison of 3C 286 with two other  $\gamma$ -ray detected

**Table 4.** X-ray variability results. 0.5–4.5 keV X-ray fluxes of 3C 286 measured with Einstein, Chandra and Swift.

date	1980-06-30	2013-02-26	2020-08-16/21
flux <sup>a</sup>	$5.3 \times 10^{-13}$	$4.0^{+0.4}_{-0.3} \times 10^{-13}$	$8.5^{+2.3}_{-2.3} \times 10^{-14}$

<sup>a</sup> corrected for Galactic absorption, in units of  $\text{erg s}^{-1}\text{cm}^{-2}$ .

NLS1 galaxies at similar redshift in Figure 4: 3C 286 has a higher flux in the optical-UV but a much lower flux in the hard X-ray band than J0946+1017 and J1222+0413.

We calculated the optical-to-X-ray spectral slope defined as  $\alpha_{\text{ox}} = -0.384 \log(f_{2\text{keV}}/f_{2500})$  (Tananbaum et al. 1979) for 3C 286 using the rest-frame flux densities at 2 keV and 2500 Å obtained from the *Swift* XRT and UVOT w1 band (effective wavelength  $\sim 2500$  Å) after  $k$ -correction. The result,  $\alpha_{\text{ox}} = 1.93$ , indicates a steep optical-to-X-ray spectral slope (Grupe et al. 2010) and relatively faint hard X-rays ( $> 1$  keV) in comparison to the optical-UV emission. This is also shown in comparison to two  $\gamma$ -ray (blazar) NLS1 galaxies, which we overplotted for comparison in Figure 4. The flatness of the X-ray spectrum itself implies the dominance of the jet emission in the hard X-ray band, likely composed of a mix of synchrotron and inverse Compton emission, as the spectral index measured with *Chandra* is steeper than the inverse Compton limit. Coronal emission from an accretion disk may contribute, too.

### 3.6 Variability

Since 3C 286 is an important calibrator source in the radio band with constant radio emission across many radio observations (Ott et al. 1994; Perley & Butler 2013a) on the one hand, but on the other hand hosts a NLS1 galaxy with a potentially highly variable accretion disk/corona system as seen in other NLS1s (Gallo 2018), we have searched for long- and short-term variability in the X-ray regime. For this, we used archival *Einstein* data, our analysis of archival *Chandra* data, and our *Swift* XRT data (Table 4).

3C 286 was observed by the *Einstein* observatory in 1980 and the flux in the 0.5–4.5 keV band corrected for Galactic absorption was reported as  $5.3 \times 10^{-13} \text{ erg s}^{-1}\text{cm}^{-2}$  (Tananbaum et al. 1983). In the same energy range, the absorption-corrected *Swift* XRT and *Chandra* fluxes were  $(8.5 \pm 2.3) \times 10^{-14} \text{ erg s}^{-1}\text{cm}^{-2}$  and  $4.0^{+0.4}_{-0.3} \times 10^{-13} \text{ erg s}^{-1}\text{cm}^{-2}$ , respectively. Even considering the large uncertainties of the *Einstein* flux, these numbers imply that the observed X-rays varied by a factor of  $\sim 4$  or higher over the past decades. As there is no evidence for absorption in the host galaxy, variability must be intrinsic and either from the accretion disk or jet. Given the evidence for  $\gamma$ -ray variability based on the *Fermi* data (Zhang et al. 2020), the variable X-rays are then most likely related to the process which also causes the  $\gamma$ -ray variability, even though an origin in the accretion-disk corona cannot be excluded at present.

### 3.7 Origin of the $\gamma$ -ray emission and NLS1-character

The majority of the  $\gamma$ -ray detected AGNs are blazars with relativistic jet directed to the observer (Abdollahi et al. 2020). Their  $\gamma$ -ray emission is produced by relativistic particles, typically electrons, in the innermost jet upscattering seed photons either from the synchrotron radiation of the jet itself (synchrotron-self-Compton process) or from the accretion disk, BLR and torus (external Compton process) (Massaro et al. 2015). Unlike blazars, radio galaxies are “misaligned” AGNs viewed at larger angle to the line of sight, and

they are interpreted as the parent population of blazars in the unification model of radio-loud AGNs (Urry & Padovani 1995). So, then the question is raised, how to produce the  $\gamma$ -ray emission in 3C 286. We address several scenarios.

First of all, it is important to note, that there is an intervening galaxy along our line of sight toward 3C 286 detected as DLA system (Section 3.1.1). We therefore wondered, whether that galaxy could instead be the counterpart to the *Fermi*-detected  $\gamma$ -ray emission. However, we can reject this scenario. First, the X-rays coincide with the optical position of 3C 286 within  $0.3''$  and no second source is detected at  $2.5''$  offset. Second, the intervening low surface brightness galaxy was found to have very low metal abundances, while any AGN/blazar is characterized by solar or even super-solar metallicity.

Next, we consider a scenario in which 3C 286 is a merger and harbors a binary SMBH; one of them accounting for the NLS1–CSS character and the other one being a blazar and producing the detected  $\gamma$ -rays. However, we do not find evidence for systematic emission-line shifts or even two systems of emission lines, and there is no evidence for excess absorption intrinsic to 3C 286 which argues against a gas-rich merger which harbors two active SMBHs.

Next, we ask if 3C 286 has an inner jet pointing at us, and responsible for strong beaming, but an outer jet bent to another direction (Massaro et al. 2015). However, from the apparent proper-motion speed, An et al. (2017) have found that the inner jet has an inclination angle to the line of sight of  $\theta = 48^\circ$  on a few tens of parsec scale, then bends at a distance of  $\sim 600$  pc. This shows, that the inner jet is still not pointing directly at us.

Next, we note that 3C 286 is not the only CSS so far detected in  $\gamma$ -rays. A few other CSSs (young and evolving radio galaxies) have also been identified as  $\gamma$ -ray emitters in recent years though their number is very low (Abdollahi et al. 2020; Zhang et al. 2020). The scenario for their  $\gamma$ -ray production is still under debate. We recall that flat radio spectrum NLS1 galaxies are actually considered as CSSs viewed at small angles (e.g., Oshlack et al. 2001; Gallo et al. 2006; Komossa et al. 2006a; Yuan et al. 2008; Bertin et al. 2016b). Therefore, the mechanism discussed in the previous papers on  $\gamma$ -ray emission of CSS can be directly applied to 3C 286, too.

For instance, it was suggested that the high energy emission up to GeV energies could be produced from the upscattered photons of an accretion disk and/or torus by relativistic electrons injected from hot spots into expanding lobes (Stawarz et al. 2008). Alternatively, the shock-accelerated particles in the young lobes could initially yield bright bremsstrahlung emission in the GeV range and then fade out (Kino et al. 2009; Kino & Asano 2011).

In particular, authors suggested that, even though faint, the  $\gamma$ -ray emission is still due to beaming of a jet at intermediate viewing angle (Kataoka et al. 2011), which leads to a lower Doppler boosting, as indeed found by modelling the broad-band SED (Zhang et al. 2020). This scenario is well possible, as long as the episodes of mild beaming do not dominate the total observed radio emission, which has been known to be so constant over some past decades. Another variant of this same scenario is, that individual jet components get occasionally deflected toward the observer as they encounter single dense blobs in the ISM along the path of the jet (Bosch-Ramon et al. 2012; Barkov et al. 2012).

Finally, it is also possible that external comptonization contributes to the  $\gamma$ -ray emission, and that it is variable because the NLS1 character of 3C 286 (low black hole mass, high Eddington ratio) leads to a strong and variable external photon field.

The last scenarios can be tested by long-term monitoring of 3C 286 with *Fermi*, along with quasi-simultaneous optical spectroscopy and SED measurements with *Swift* and in the VLBI radio regime.

## 4 SUMMARY AND CONCLUSIONS

We have carefully established the NLS1 character of 3C 286 based on its full UV-optical spectrum and multi-wavelength data, and based on a variety of measurements and considerations which go far beyond a simple FWHM measurement. Of particular importance for the source classification was evaluating complexity in the [O III] line implying a strong outflow component, not seen in Mg II however, as well as the multiple lines of evidence for a lack of significant dust extinction towards 3C 286 and the lack of intrinsic absorption.

The simultaneous optical–UV–X-ray SED implies a strong accretion-disk component in the EUV, consistent with emission-line ratio diagnostics ([O II]/[O III] in combination with [Ne III]/[Ne V]).

With a SMBH mass of order  $10^8 M_\odot$ , 3C 286 is at the high-mass range of NLS1 galaxies, and at the low-mass end of radio-loud BLS1 galaxies. It is accreting near the Eddington limit, which may explain the strong outflow component we detect in all high-ionization emission lines.

3C 286 is the radio-loudest  $\gamma$ -ray emitting NLS1 galaxy identified so far, with a radio loudness of  $\log R = 4.4$ , and one of the radio-loudest systems known.

Our detection of high-amplitude X-ray variability (plausibly associated with those jet-component(s) which also emit the  $\gamma$ -rays) suggests caution when using 3C 286 as radio calibrator in highest-resolution radio VLBI observations.

While 3C 286 is not an EHT calibrator as it is too extended, it would become an interesting primary target in the future, if the flaring in X-rays and  $\gamma$ -rays re-occurs.

## ACKNOWLEDGEMENTS

We would like to thank the *Swift* team for carrying out our observations, and Jose L. Gómez for very useful discussions. Su Yao acknowledges support by an Alexander von Humboldt Foundation Fellowship. This work has made use of the data products from SDSS, *Swift* and *Chandra*. This work has also made use of the NASA Astrophysics Data System Abstract Service (ADS), and the NASA/IPAC Extragalactic Database (NED) which is operated by the Jet Propulsion Laboratory, California Institute of Technology, under contract with the National Aeronautics and Space Administration.

Funding for the SDSS IV has been provided by the Alfred P. Sloan Foundation, the U.S. Department of Energy Office of Science, and the Participating Institutions. SDSS-IV acknowledges support and resources from the Center for High Performance Computing at the University of Utah. The SDSS website is www.sdss.org. SDSS-IV is managed by the Astrophysical Research Consortium for the Participating Institutions of the SDSS Collaboration including the Brazilian Participation Group, the Carnegie Institution for Science, Carnegie Mellon University, Center for Astrophysics | Harvard & Smithsonian, the Chilean Participation Group, the French Participation Group, Instituto de Astrofísica de Canarias, The Johns Hopkins University, Kavli Institute for the Physics and Mathematics of the Universe (IPMU) / University of Tokyo, the Korean Participation Group, Lawrence Berkeley National Laboratory, Leibniz Institut für Astrophysik Potsdam (AIP), Max-Planck-Institut für Astronomie (MPIA Heidelberg), Max-Planck-Institut für Astrophysik (MPA Garching), Max-Planck-Institut für Extraterrestrische Physik (MPE), National Astronomical Observatories of China, New Mexico State University, New York University, University of Notre Dame, Observatório Nacional / MCTI, The Ohio State University, Pennsylvania State University, Shanghai Astronomical Observatory, United Kingdom

Participation Group, Universidad Nacional Autónoma de México, University of Arizona, University of Colorado Boulder, University of Oxford, University of Portsmouth, University of Utah, University of Virginia, University of Washington, University of Wisconsin, Vanderbilt University, and Yale University.

## DATA AVAILABILITY

The data underlying this article are available in the SDSS archive at <https://dr16.sdss.org/optical/spectrum/search>, the astronomical archives of the HEASARC at <https://heasarc.gsfc.nasa.gov/docs/archive.html>, the *Swift* archive at <https://swift.gsfc.nasa.gov/archive/> and the *Chandra* data archive at <https://cda.harvard.edu/chaser/>, and can be accessed with the source coordinates or observation IDs.

## REFERENCES

- Abdo A. A., et al., 2009, *ApJ*, 707, L142
- Abdollahi S., et al., 2020, *ApJS*, 247, 33
- Agudo I., Thum C., Gómez J. L., Wiesemeyer H., 2014, *A&A*, 566, A59
- Akujor C. E., Garrington S. T., 1995, *A&AS*, 112, 235
- An T., Hong X.-Y., Wang W.-H., 2004, *Chinese J. Astron. Astrophys.*, 4, 28
- An T., Lao B. Q., Zhao W., Mohan P., Cheng X. P., Cui Y. Z., Zhang Z. L., 2017, *MNRAS*, 466, 952
- Arnaud K. A., 1996, in Jacoby G. H., Barnes J., eds, *Astronomical Society of the Pacific Conference Series Vol. 101, Astronomical Data Analysis Software and Systems V*. p. 17
- Aslanian A. M., Dagkesamanskii R. D., Kozhukhov V. N., Malumian V. G., Sanamian V. A., 1968, *Astrofizika*, 4, 129
- Barkov M. V., Bosch-Ramon V., Aharonian F. A., 2012, *ApJ*, 755, 170
- Becker R. H., White R. L., Helfand D. J., 1995, *ApJ*, 450, 559
- Berton M., Foschini L., Ciroi S., Cracco V., La Mura G., Di Mille F., Rafanelli P., 2016a, *A&A*, 591, A88
- Berton M., et al., 2016b, *A&A*, 591, A98
- Berton M., et al., 2017, *Frontiers in Astronomy and Space Sciences*, 4, 8
- Boisse P., Le Brun V., Bergeron J., Deharveng J.-M., 1998, *A&A*, 333, 841
- Boroson T. A., Green R. F., 1992, *ApJS*, 80, 109
- Bosch-Ramon V., Perucho M., Barkov M. V., 2012, *A&A*, 539, A69
- Breeveld A. A., et al., 2010, *MNRAS*, 406, 1687
- Brown A. M., Adams J., 2012, *MNRAS*, 421, 2303
- Brown R. L., Roberts M. S., 1973, *ApJ*, 184, L7
- Burrows D. N., et al., 2005, *Space Sci. Rev.*, 120, 165
- Cash W., 1979, *ApJ*, 228, 939
- Chandra P., Ray A., Bhatnagar S., 2004, *ApJ*, 612, 974
- Chen X., Wright E. L., 2009, *ApJ*, 694, 222
- Cleary K., Lawrence C. R., Marshall J. A., Hao L., Meier D., 2007, *ApJ*, 660, 117
- Cohen R. D., Barlow T. A., Beaver E. A., Junkkarinen V. T., Lyons R. W., Smith H. E., 1994, *ApJ*, 421, 453
- Cohen A. S., Lane W. M., Cotton W. D., Kassim N. E., Lazio T. J. W., Perley R. A., Condon J. J., Erickson W. C., 2007, *AJ*, 134, 1245
- Cotton W. D., Fanti C., Fanti R., Dallacasa D., Foley A. R., Schilizzi R. T., Spencer R. E., 1997, *A&A*, 325, 479
- Curran S. J., Murphy M. T., Pihlström Y. M., Webb J. K., Bolatto A. D., Bower G. C., 2004, *MNRAS*, 352, 563
- Cutri R. M., et al., 2013, *Explanatory Supplement to the AllWISE Data Release Products, Explanatory Supplement to the AllWISE Data Release Products*
- Dawson K. S., et al., 2013, *AJ*, 145, 10
- Ferrarese L., Ford H., 2005, *Space Sci. Rev.*, 116, 523
- Fomalont E. B., Frey S., Paragi Z., Gurvits L. I., Scott W. K., Taylor A. R., Edwards P. G., Hirabayashi H., 2000, *ApJS*, 131, 95
- Foschini L., et al., 2015, *A&A*, 575, A13
- Gabányi K. É., et al., 2007, *A&A*, 470, 83
- Gallo L., 2018, in *Revisiting Narrow-Line Seyfert 1 Galaxies and their Place in the Universe*. p. 34 ([arXiv:1807.09838](https://arxiv.org/abs/1807.09838))
- Gallo L. C., et al., 2006, *MNRAS*, 370, 245
- Gehrels N., et al., 2004, *ApJ*, 611, 1005
- Gelderman R., Whittle M., 1994, *ApJS*, 91, 491
- Gold B., et al., 2011, *ApJS*, 192, 15
- Grasha K., Darling J., Bolatto A., Leroy A. K., Stocke J. T., 2019, *ApJS*, 245, 3
- Gregory P. C., Condon J. J., 1991, *ApJS*, 75, 1011
- Griffin R. D., Dai X., Thompson T. A., 2016, *ApJ*, 823, L17
- Grupe D., Mathur S., 2004, *ApJ*, 606, L41
- Grupe D., Komossa S., Leighly K. M., Page K. L., 2010, *ApJS*, 187, 64
- HI4PI Collaboration et al., 2016, *A&A*, 594, A116
- Hayashida M., et al., 2013, *ApJ*, 779, 131
- Hill J. E., et al., 2004, in Flanagan K. A., Siegmund O. H. W., eds, *Society of Photo-Optical Instrumentation Engineers (SPIE) Conference Series Vol. 5165, X-Ray and Gamma-Ray Instrumentation for Astronomy XIII*. pp 217–231, [doi:10.1117/12.505728](https://doi.org/10.1117/12.505728)
- Hirst P., Jackson N., Rawlings S., 2003, *MNRAS*, 346, 1009
- Jenness T., Robson E. I., Stevens J. A., 2010, *MNRAS*, 401, 1240
- Kataoka J., et al., 2011, *ApJ*, 740, 29
- Kellermann K. I., Sramek R., Schmidt M., Shaffer D. B., Green R., 1989, *AJ*, 98, 1195
- Kino M., Asano K., 2011, *MNRAS*, 412, L20
- Kino M., Ito H., Kawakatu N., Nagai H., 2009, *MNRAS*, 395, L43
- Komossa S., 2008, in *Revista Mexicana de Astronomía y Astrofísica Conference Series*, 32. pp 86–92 ([arXiv:0710.3326](https://arxiv.org/abs/0710.3326))
- Komossa S., 2018, in *Revisiting Narrow-Line Seyfert 1 Galaxies and their Place in the Universe*. p. 15 ([arXiv:1807.03666](https://arxiv.org/abs/1807.03666))
- Komossa S., Xu D., 2007, *ApJ*, 667, L33
- Komossa S., Voges W., Xu D., Mathur S., Adorf H.-M., Lemson G., Duschl W. J., Grupe D., 2006a, *AJ*, 132, 531
- Komossa S., Voges W., Adorf H.-M., Xu D., Mathur S., Anderson S. F., 2006b, *ApJ*, 639, 710
- Komossa S., Xu D., Zhou H., Storchi-Bergmann T., Binette L., 2008, *ApJ*, 680, 926
- Komossa S., et al., 2015, *A&A*, 574, A121
- Komossa S., Xu D. W., Wagner A. Y., 2018, *MNRAS*, 477, 5115
- Kuehr H., Witzel A., Pauliny-Toth I. I. K., Nauber U., 1981, *A&AS*, 45, 367
- Laing R. A., Peacock J. A., 1980, *MNRAS*, 190, 903
- Laor A., Jannuzi B. T., Green R. F., Boroson T. A., 1997, *ApJ*, 489, 656
- Laurent-Muehleisen S. A., Kollgaard R. I., Ryan P. J., Feigelson E. D., Brinkmann W., Siebert J., 1997, *A&AS*, 122, 235
- Liao M., Gu M., 2020, *MNRAS*, 491, 92
- Lipari S., Colina L., Macchetto F., 1994, *ApJ*, 427, 174
- Mainzer A., et al., 2011, *ApJ*, 731, 53
- Mantovani F., Mack K. H., Montenegro-Montes F. M., Rossetti A., Kraus A., 2009, *A&A*, 502, 61
- Mao S. A., Gaensler B. M., Haverkorn M., Zweibel E. G., Madsen G. J., McClure-Griffiths N. M., Shukurov A., Kronberg P. P., 2010, *ApJ*, 714, 1170
- Markwardt C. B., 2009, in Bohlender D. A., Durand D., Dowler P., eds, *Astronomical Society of the Pacific Conference Series Vol. 411, Astronomical Data Analysis Software and Systems XVIII*. p. 251 ([arXiv:0902.2850](https://arxiv.org/abs/0902.2850))
- Massaro F., Thompson D. J., Ferrara E. C., 2015, *A&ARv*, 24, 2
- McLure R. J., Dunlop J. S., 2004, *MNRAS*, 352, 1390
- Meisenheimer K., Haas M., Müller S. A. H., Chini R., Klaas U., Lemke D., 2001, *A&A*, 372, 719
- Meyer D. M., York D. G., 1992, *ApJ*, 399, L121
- Nelson C. H., 2000, *ApJ*, 544, L91
- Oshlack A. Y. K. N., Webster R. L., Whiting M. T., 2001, *ApJ*, 558, 578
- Osterbrock D. E., Ferland G. J., 2006, *Astrophysics of gaseous nebulae and active galactic nuclei*. University Science Books
- Ott M., Witzel A., Quirrenbach A., Krichbaum T. P., Standke K. J., Schalinski C. J., Hummel C. A., 1994, *A&A*, 284, 331

- Paliya V. S., Ajello M., Rakshit S., Mandal A. K., Stalin C. S., Kaur A., Hartmann D., 2018, *ApJ*, **853**, L2
- Peacock J. A., Wall J. V., 1982, *MNRAS*, **198**, 843
- Pei Y. C., Fall S. M., Bechtold J., 1991, *ApJ*, **378**, 6
- Peng F.-K., Wang X.-Y., Liu R.-Y., Tang Q.-W., Wang J.-F., 2016, *ApJ*, **821**, L20
- Perley R. A., Butler B. J., 2013a, *ApJS*, **204**, 19
- Perley R. A., Butler B. J., 2013b, *ApJS*, **206**, 16
- Pettini M., King D. L., Smith L. J., Hunstead R. W., 1997, *ApJ*, **478**, 536
- Poole T. S., et al., 2008, *MNRAS*, **383**, 627
- Raiteri C. M., et al., 2010, *A&A*, **524**, A43
- Richards J. L., et al., 2011, *ApJS*, **194**, 29
- Roming P. W. A., et al., 2005, *Space Sci. Rev.*, **120**, 95
- Schlafly E. F., Finkbeiner D. P., 2011, *ApJ*, **737**, 103
- Shen Y., et al., 2011, *ApJS*, **194**, 45
- Sikora M., Stawarz Ł., Lasota J.-P., 2007, *ApJ*, **658**, 815
- Simon R. S., Readhead A. C. S., Moffet A. T., Wilkinson P. N., Anderson B., 1980, *ApJ*, **236**, 707
- Skrutskie M. F., et al., 2006, *AJ*, **131**, 1163
- Spencer R. E., McDowell J. C., Charlesworth M., Fanti C., Parma P., Peacock J. A., 1989, *MNRAS*, **240**, 657
- Stawarz Ł., Ostorero L., Begelman M. C., Moderski R., Kataoka J., Wagner S., 2008, *ApJ*, **680**, 911
- Steidel C. C., Pettini M., Dickinson M., Persson S. E., 1994, *AJ*, **108**, 2046
- Sulentic J. W., Zwitter T., Marziani P., Dultzin-Hacyan D., 2000, *ApJ*, **536**, L5
- Tananbaum H., et al., 1979, *ApJ*, **234**, L9
- Tananbaum H., Wardle J. F. C., Zamorani G., Avni Y., 1983, *ApJ*, **268**, 60
- Tsuzuki Y., Kawara K., Yoshii Y., Oyabu S., Tanabé T., Matsuoka Y., 2006, *ApJ*, **650**, 57
- Urry C. M., Padovani P., 1995, *PASP*, **107**, 803
- Vanden Berk D. E., et al., 2001, *AJ*, **122**, 549
- Véron-Cetty M. P., Véron P., 2010, *A&A*, **518**, A10
- Véron-Cetty M.-P., Joly M., Véron P., 2004, *A&A*, **417**, 515
- Vestergaard M., Peterson B. M., 2006, *ApJ*, **641**, 689
- Waldram E. M., Yates J. A., Riley J. M., Warner P. J., 1996, *MNRAS*, **282**, 779
- Wang J.-G., et al., 2009, *ApJ*, **707**, 1334
- Wilkinson P. N., Readhead A. C. S., Anderson B., Purcell G. H., 1979, *ApJ*, **232**, 365
- Wolfe A. M., Broderick J. J., Condon J. J., Johnston K. J., 1976, *ApJ*, **208**, L47
- Wolfe A. M., Jorgenson R. A., Robishaw T., Heiles C., Prochaska J. X., 2008, *Nature*, **455**, 638
- Wright E. L., 2006, *PASP*, **118**, 1711
- Wright E. L., et al., 2010, *AJ*, **140**, 1868
- Xu D., Komossa S., Zhou H., Lu H., Li C., Grupe D., Wang J., Yuan W., 2012, *AJ*, **143**, 83
- Yao S., 2016, PhD thesis, National Astronomical Observatories of China, CAS, [https://www.nstl.gov.cn/paper\\_detail.html?id=9477edc12f86fc382e8c24101223f33c](https://www.nstl.gov.cn/paper_detail.html?id=9477edc12f86fc382e8c24101223f33c)
- Yao S., Yuan W., Zhou H., Komossa S., Zhang J., Qiao E., Liu B., 2015, *MNRAS*, **454**, L16
- Yao S., Komossa S., Liu W.-J., Yi W., Yuan W., Zhou H., Wu X.-B., 2019, *MNRAS*, **487**, L40
- York D. G., et al., 2000, *AJ*, **120**, 1579
- Yuan W., Zhou H. Y., Komossa S., Dong X. B., Wang T. G., Lu H. L., Bai J. M., 2008, *ApJ*, **685**, 801
- Zhang J., Zhang H.-M., Gan Y.-Y., Yi T.-F., Wang J.-F., Liang E.-W., 2020, *ApJ*, **899**, 2
- Zhou H., Wang T., Yuan W., Lu H., Dong X., Wang J., Lu Y., 2006, *ApJS*, **166**, 128

This paper has been typeset from a  $\text{\TeX}/\text{\LaTeX}$  file prepared by the author.